The running-in tribological behavior of Pb-free brass and its effect on microstructural evolution

Lin Liu [a, d, *1], Zhichen Zhang [a, d], Martin Dienwiebel [b, c, *2]

[a] School of Mechanical Engineering, Changzhou University, 213164 Changzhou, Jiangsu, China

[b] Karlsruhe Institute for Technology, Institute for Applied Materials, Kaiserstraße 12, 76128 Karlsruhe, Germany

[c] Fraunhofer Institute for Mechanics of Materials IWM, Wöhlerstraße 11, 79108 Freiburg, Germany

[d] Jiangsu Key Laboratory of Green Process Equipment, Changzhou University, 213164 Changzhou, Jiangsu, China

Highlights

- Characterization of running-in under boundary lubrication conditions.
- Transfer and adhesive wear in the initial phase.
- Microstructural evolution due to dislocation movement promotion during the test.
- A grain refinement mechanism during sliding experiment is proposed.

ABSTRACT

In this paper, the running-in tribological behavior of Pb-free brass (i.e. 64% copper and 36% Zinc) sliding against 100Cr6 under lubricated condition and its effect on grain refinement are investigated systematically. The sliding experiment is preformed using a tribometer based on in-situ holography microscopy and radionuclide technique. After the tribological test, the friction pair are characterized using scanning electron microscopy (SEM), and transmission electron microscopy (TEM) in order to quantify the micrography, chemistry, and microstructure.

It is found that the curve of the friction coefficient (COF) exhibits two steep falls during the initial stage, while the real-time wear rates at these moments are relatively high. Then the test enters the dynamic stability stage due to equilibrium between the processes of strain hardening and recovery. The brass sliding experiment is carried out in the boundary lubrication region leading to dislocation movement and void formation due to plastic deformation. Moreover, an exceptional increase in two directional stacking faults is observed that extend and interdiffuse into each other. More importantly, as has been observed before, the coarse grains are considerably refined into nano-grains due to the accumulation of dislocation movement induced by repeated sliding test.

Keywords: tribological behavior, dislocation transitions, grain refinement, copper-zinc alloy

1. Introduction

Copper and its alloys characterized by excellent workability, high thermal conductivity and

[*1] Corresponding author at: School of Mechanical Engineering of Changzhou University, Gehu Road 1, 213164 Changzhou, Jiangsu, China. Tel.: +86 519 81169803; fax: +86 519 81169810.
E-mail address: liulin@cczu.edu.cn (Lin Liu).

[*2] Corresponding author at: Karlsruhe Institute for Technology, Institute for Applied Materials, Kaiserstraße 12, 76128 Karlsruhe, Germany. Tel.: +49 721 4640751; fax: +49 7216084364.
E-mail address: martin.dienwiebel@kit.edu (Martin Dienwiebel).

electrical conductivity, as well as exceptional wear resistance property are therefore widely used for applications in machinery parts [1-5]. The addition of lead (Pb) to the copper alloy can improve its wear resistance [6], whereas the use of copper alloys with lead added, which will cause serious pollution to the environment, is still restricted by laws in recent years [7-10]. Accordingly, Pb-free copper alloys are focused by researchers because of their environmentally friendly performance and excellent mechanical comprehensive behaviors.

All the time, most studies have focused on steady-state conditions and only a few have paid attention to the running-in behavior [5]. However, the process tribological data (i.e. topography, roughness, and real-time wear rate etc.), which are obtained during the running-in stage, play important roles in understanding friction and wear mechanism. Moreover, it is beneficial in order to control low friction and high endurance life [11-13].

The purpose of this research is to investigate the tribological behavior of Pb-free brass (CuZn36) and its grain refinement mechanism during the experiment. The topographical behavior and real-time wear rate of brass were studied using an in-situ tribometer, while the morphology and the chemical composition of the wear track were analyzed by scanning electron microscopy (SEM). In addition, the microstructure of the wear track was investigated by means of transmission electron microscopy (TEM).

2. Experimental Procedure

2.1 Characterization techniques

A scanning electron microscope (JSM-6510) is used to examine the friction pair morphology of brass. To analyze the wear track microstructure of brass, the TEM samples are prepared and then observed by JEOL-2100 transmission electron microscope.

2.2 Sample preparation

For the tribological experiments, 100Cr6 spheres with diameter of Ø2mm (0.9~1.05%C, 1.35~1.65%Cr) are used as counter material. The spheres are first hand-grinded and then hand-polished on one side in order to obtain flat-on-flat geometry. The diameter of the flat contact varied between 1.71 and 2.20 mm. The Vickers hardness and Young's modulus of the pins are measured to be 830 ± 10.3HV and 210GPa respectively (Shimadzu HMV-2000). The brass plates (63.9%Cu, 36.1%Zn) with a size of 150×75×4 mm^3 are annealed at a temperature of 650 ℃ for 45 min to homogenize the composition and eliminate the residual stress. In order to remove the effect of oxide layer created during annealing, the brass plates are cleaned with citric acid. The average roughness values (Ra) of the plates and the pins after being polished are measured to be 14nm and 120nm, respectively. Surface of brass plates are labeled by radionuclides (Zn65) in order to measure real-time wear of the alloy with nanometer resolution by radionuclide technique (RNT) [14,15].

In order to obtain the microstructure of wear surface, preliminary preparation technique is applied. The plate-samples are first hand-grinded with 2500 grits of abrasive paper, and then the samples are grinded by the disc grinder (Gatan-623) until its thickness reaches 60~100μm. Subsequently, the samples are chemistry-milled by the twin-jet electro-polisher (TenuPol-5) with appropriate electrolyte. Two plate-samples with wear track are bonded face-to-face to protect the worn surface during chemistry-milled in particular [16].

2.3 Tribological experiment

The tribological experiments are performed using an in-situ tribometer based on in-situ

holographic microscopy and radionuclide technique. It consists of a force sensor, holographic microscope, an atomic force microscope, and a RNT chamber. Every part can be used individually or together in one experiment. For this study we only used the force sensor, the holographic microscope, and the RNT chamber. The microstructure evolution of friction surface during the test is investigated by in-situ holographic microscopy. Meanwhile, the real-time wear is measured by RNT chamber. More details on the design of the tribometer can be found in [17]. All sliding experiments are performed at room temperature (T=25 ℃) and a relative approximately 50% RH. The experiments are conducted in lubricating conditions using transparent base oil poly-alpha olefin (PAO-8) with viscosity of 45.8 mm^2/s at 40 ℃. During the experiments, the oil temperature is kept at 35 ℃ controlling by a Julabo HE-4 pumping system. The experimental path is linear reciprocating with a length of 120 mm. 18 groups are conducted with the velocity of sliding experiments being 20 mm/s, while the contact pressures range from 1.5MPa to 8.0MPa. Each group is repeated three times under the same conditions in order to obtain the consistent results.

3. Results

3.1 Tribological behavior

It is observed that the lowest friction and scatter in the values, is only obtained with a contact pressure between 1.9 and 3.0 MPa. One of the typical experiments (contact pressure 2.5MPa) with “good running-in behaviors” was chosen to investigate the running-in tribological behavior of brass and its effect on the grain refinement.

The evolution of the COF, wear rate and roughness with respect to the number of cycles are illustrated in Fig.1 (a). The characteristic topography images correspond to specific cycles are selected and shown in Fig.1 (b).

Initially, the COF raises at a fast rate reaching a maximum 0.317 at 461 cycles. Afterwards the COF steeply drops to a value below 0.20. While the real-time wear rate increases to 1.054 mg/30min along with the friction coefficient dropping. The friction remains relatively stable showing some peaks (i.e. μ=0.285 at 1032 cycles). From 1032 to 2000 cycles, the COF decreases gradually and then increases slightly again at 1479 cycles, while the wear rate increases to a maximum of 2.0 mg/30min at this moment. After 2000 cycles, the COF remains stable at around 0.20 and oscillates between 0.17 and 0.23 slightly for the remaining cycle numbers, in the meantime the experiment shows a significant decrease in wear rate with considerably smaller scatter in the value and remain constant for the remaining cycles.

The trend of COF curve and roughness curve are matched well except for few periods of cycles. Initially, the average roughness R_a is low (< 20 nm) but then increases (> 40 nm) significantly after a few cycles. From 100 to 2500 cycles R_a oscillates between 30 and 40 nm, and then Ra is relatively stable for the remainder of the test.

The topographical changes of the wear track throughout the sliding are monitored using the DHM attached to the in-situ tribometer. Fig. 1(b) contains images that are taken from six different typical cycles of the sliding experiments. With the beginning of the test, the smoothness of the surface is quickly destroyed being accompanied by a significant amount of debris particles [18] (e.g. 400). At about 500 to 2000 cycles, the surface topography of the experiment oscillates between being rough (e.g. 500 and 1500) and being smooth (e.g. 1400) with the presence of debris particles. After the 2000th cycle, however, the topography for wear track appears smoother again.

For the remainder of the test, the surface topography of the test shows a significantly smoother surface without any obvious changes for the remaining cycles.

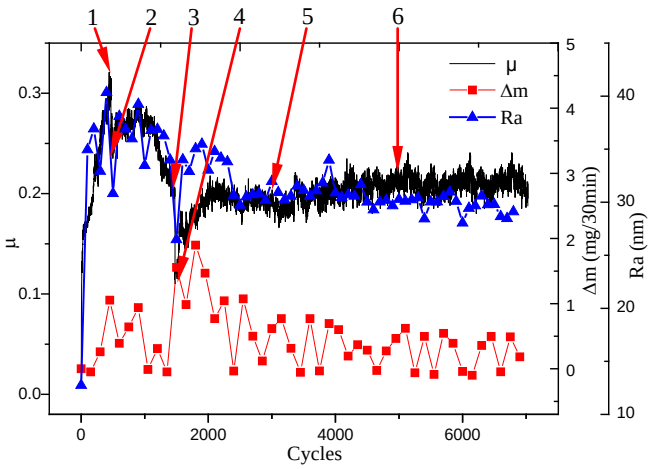

(a)

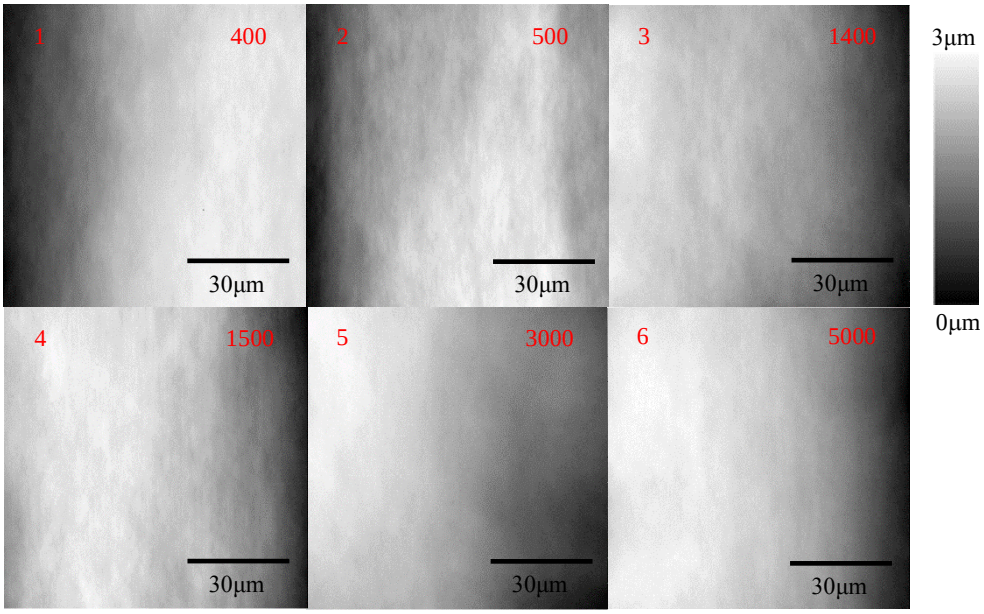

(b)

Fig.1. Coefficient of friction, wear rate and roughness *vs*. cycles (a). Characteristic topography images that correspond to specific cycles which indicated by arrows and numbers are depicted below (b).

3.2 Micrography

Fig. 2 shows the micrographs of brass and pin after the test under the scanning electron microscopy. The narrow wear track parallel to the sliding direction with furrows and pits are observed. Obviously, adhesive wear occurs during the experiment with the white stripes sticking on the surface of the pin (Fig. 2(c)).

Table 1 Chemical composition of different zone by EDS analysis

Spectrum	Fe	Cu	Zn
Spectrum 1	6.9	77.5	15.5

Spectrum 2	96.3	3.2	0.5
Spectrum 3	92.1	6.8	1.1
Spectrum 4	8.4	77.0	14.7
Average	50.9	41.1	8.0
Standard deviation	43.3	36.1	7.2
Maximum	96.3	77.5	15.5
Minimum	6.9	3.2	0.5

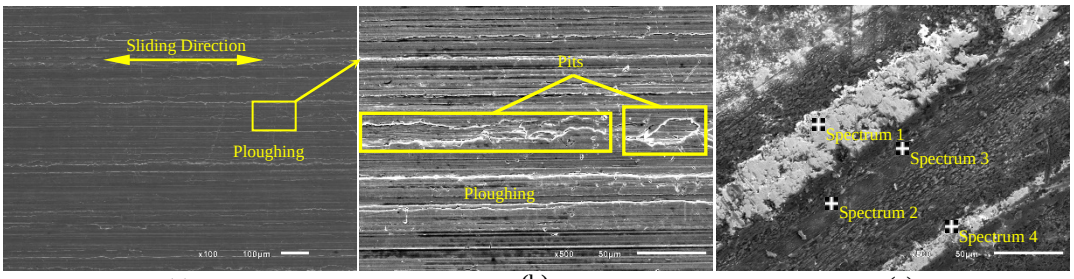

(a) (b) (c)

Fig.2 SEM micrograph characterizes of the friction pair for wear track (a, b) and pin (c).

In order to determine the chemical composition of the white stripes, the EDS analysis of the pin is obtained using the SEM. Table 1 shows chemical composition of the investigated zones (Fig. 2(c)). The main component of the black zones areas is iron, while the main components of the white stripe areas are copper and zinc. It is established that adhesive wear causes brass to transfer to the pin.

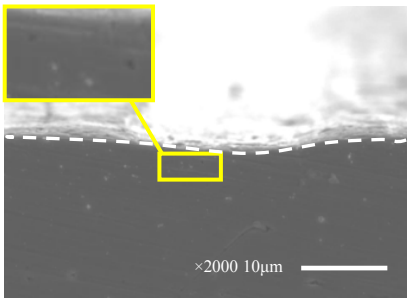

Fig.3 SEM cross-section perpendicular to the wear track.

Cross-sectional SEM cuts perpendicular to the wear track is performed in order to gain insight on the subsurface micrograph. Several voids are observed with spatial distribution near the worn surface.

3.3 Microstructure

TEM observations of the wear track are shown in Fig. 4, Fig. 5 and Fig. 6. Two different shear bands (SB1 and SB2) are observed in Fig. 4(a), while the SB1, which is more distinct than the SB2, is parallel to the sliding direction of the test. In addition, the SB2 has a certain angle with the SB1. Moreover, stacking fault 1 (SF1) and stacking fault 2 (SF2), which are almost parallel to the longitudinal direction of SB1 and SB2 respectively, are found in Fig. 4(b). Various dislocation structures (dislocation tangles (DT), dislocation cells (DC) and dislocation walls (DW)) as an effect of plastic deformation due to sliding test (Fig. 5) are observed. It can also be seen that the accumulation of dislocation structures (DT, DC, DW, etc.) contributes to the formation of nano-size grains (Fig. 6: i.e. 5-50 nm).

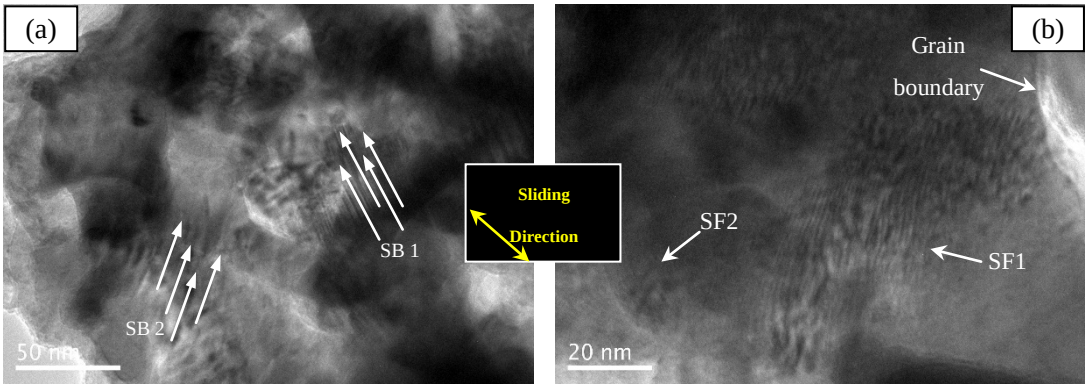

Fig.4 TEM images of the wear track; (a) shear bands (SB), (b) stacking faults (SF)

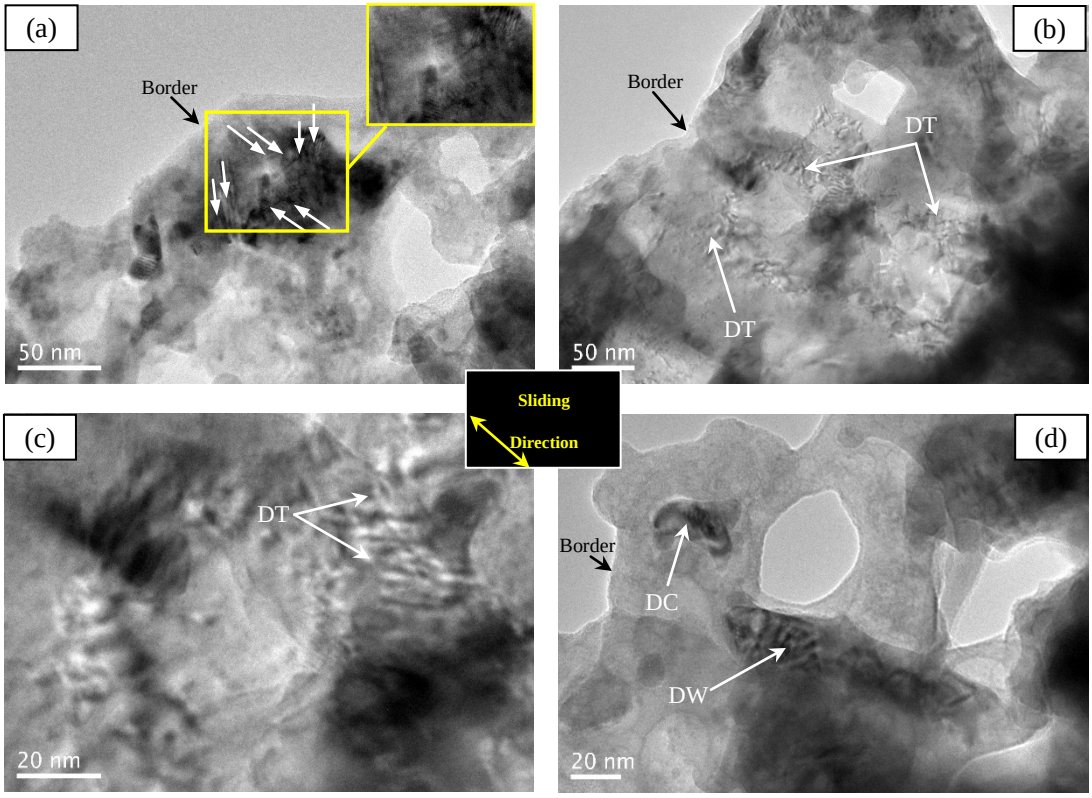

Fig.5 TEM-images of the wear track; (a) interaction of different shear bands and stacking faults, (b) and (c) dislocation tangles (DT), (d) dislocation cells (DC) and dislocation walls (DW).

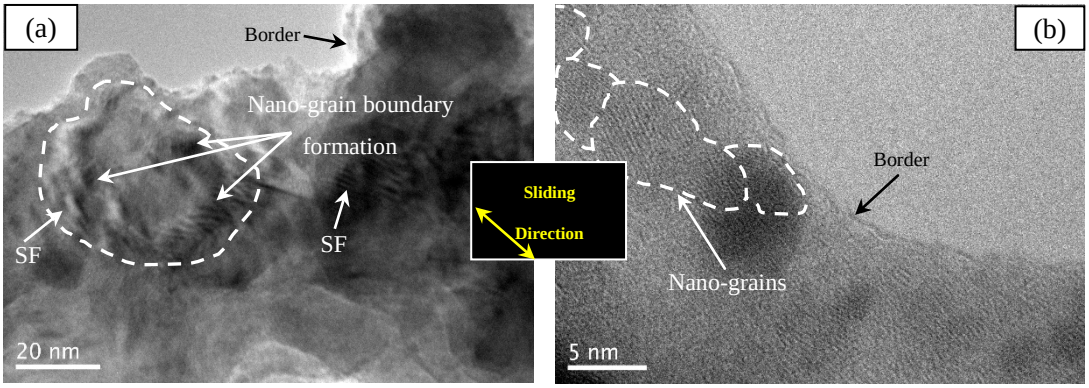

Fig.6 TEM-images of the wear track; (a) nano-grain boundary formation and stacking faults (SF), (b) nano-grain structures.

4. Discussion

In the beginning of the test, the COF and roughness increase speedy (Fig. 1(a)), while the value of wear rate is relative low. Such phenomena means that the initial dislocation movement induced by sliding causes plastic deformation of original grains [19]. The dislocation movement accumulates with the sliding, and then several dislocation pile-ups generates in areas. The main reason of low wear rate along with sharp increasing of the COF and roughness in the beginning is that most of the dislocation pile-ups do not accumulate to the critical limit, which causes the debris particles peeling off [20]. It is noticeable that two steep falls are shown on the curve of the COF and roughness at approximately 460 cycles and 1480 cycles respectively, whereas the real-time wear rates at the moment are relatively high. Accordingly, it can be inferred that the COF is special related to the real-time wear rate in the initial stage. The numbers of dislocation pile-ups accumulate to the limit, which involves voids and original cracks on the wear track, as the test continuing. The original cracks continues to grow that causes the number of debris particles increased rapidly, based on delamination theory [21]. Lubricant invades the pits and the furrows, which are generated by the formation of debris particles at the movement of test, on the wear track to cause the COF to decrease. In addition, the roughness curve (Fig. 1(a)) and topography images (Fig. 1(b)) are in good agreement with the phenomenon of relationship between COF and real-time wear rate in the initial stage.

After approximately 2000 cycles, COF, roughness and real-time wear rate enter the dynamic stability stage with the accumulation of plastic deformation in surface layer. Such phenomenon is apparently supported by the viewpoint of Moshkovich and Perfilyev et al.[22], who believe that the dynamic stability stage is mainly responsible for the equilibrium between the processes of strain hardening and recovery. In the dynamic stability stage, the wear resistance layer with nano-grains (Fig. 6) is formed, thereby inducing the values of COF, roughness and wear rate remaining stable and low. Such phenomenon supports that the original grains on the worn surface refine during the sliding test. The grain refinement restrains dislocation movement inside the grain, reflecting the strain hardening on the worn surface.

Determining the lubrication region of brass during the test is important for understanding its tribological behavior. According to Moshkovich et al. [22-24], the lubrication number of Schipper, $Z=\eta \bullet v/p \bullet Ra$, is used as the horizontal axis of the Stribeck curve. Here, η is the viscosity of the lubricant, v is the sliding velocity, p is the pressure and Ra is the arithmetic mean of the departures of the profile from the mean line for the harder sample. For this experiment, the calculated Schipper value is 3.05×10^{-6}, which is lower than the critical value between the boundary lubrication region and mixed lubrication region. Therefore, it can be seen that the test is in the boundary lubrication region. Several furrows and pits on the wear track are observed after experiment (Fig. 2(a) and Fig. 2(b)). Moreover, the SEM-EDS analysis (Fig. 2(c) and Table 1) confirms that adhesive wear occurs during the experiment. As stated above, it can be inferred that the brass friction in the boundary lubrication region is accompanied by adhesive wear.

A significant amount of debris particles (Fig. 1(b)) are observed during the test. The delamination theory, which interprets the cause of debris particles, proposed by Suh [21] suggests that the debris particles originate from the behavior of dislocation at the surface, sub-surface crack and void formation. As a result of the sliding test, severe shear plastic deformation generates and accumulates dislocation, which give rise to cracks and voids (Fig. 3) in the surface layer of brass.

The primary and subsidiary slip systems are found in Fig. 4(a). As previously reported by Moshkovich et al., the formation and distribution of voids can be probably initiated by the intersection between primary and subsidiary slip systems due to the work hardening [25]. Furthermore, the void distribution in the sub-surface accelerates the accumulation of dislocation near the surface [21]. Consequently, there is a mutual promotion between dislocation movement and void formation during the sliding test.

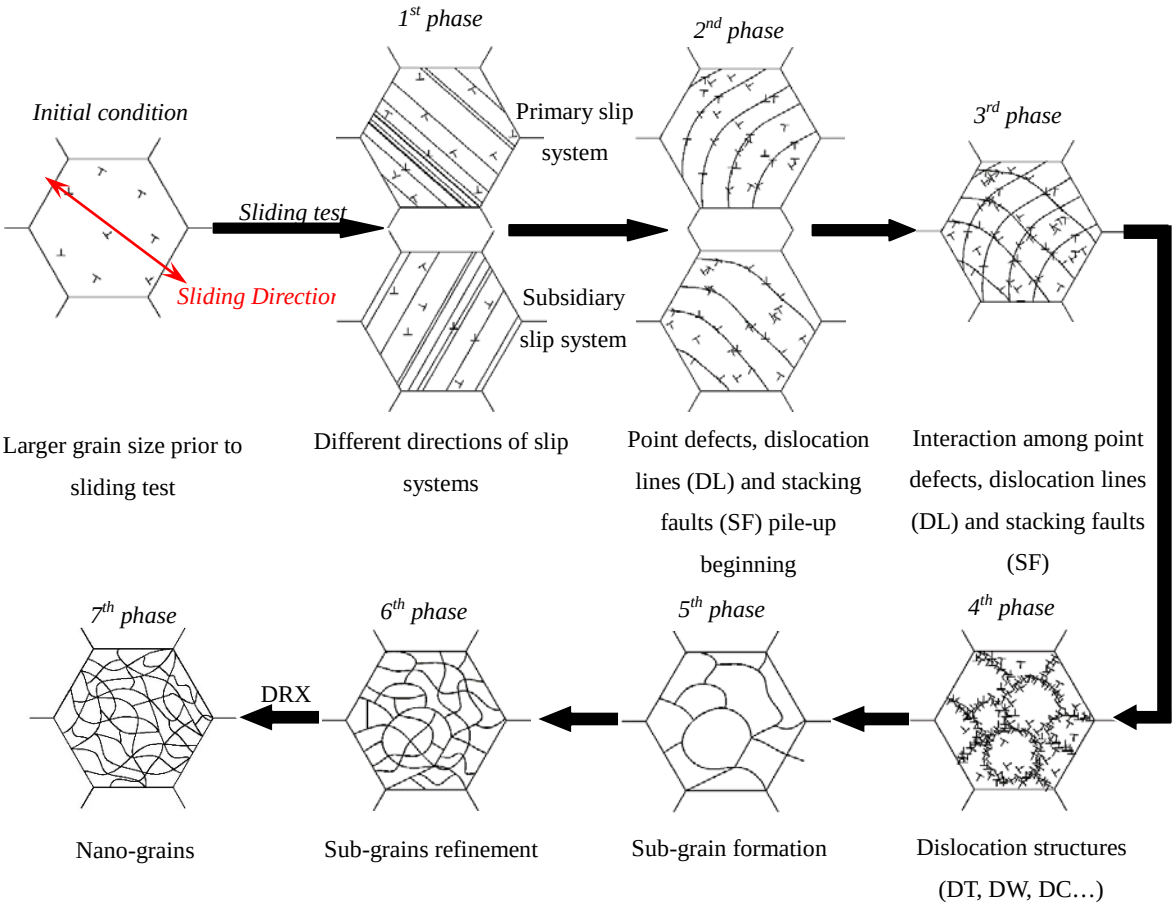

Fig.7 Proposed schematic presentation of the grain refinement mechanism of brass during sliding experiment

A schematic presentation of the grain refinement mechanism of brass during sliding experiment, based on the above TEM microstructure analysis and the method of mechanism analysis in Ref.[26], is presented in Fig.7. The grain refinement probably occurs in the following sequence:

(I). In the 1st phase, the continuous action of sliding friction, which are propagating into material cause initial accumulation of dislocation movement, reflecting in the generation of two different directions of slip systems with SB1 and SB2 (Fig. 4(a)). It is noteworthy at this point that the direction of SB1, which is more observable than SB2, is parallel to the sliding direction. Based on the above phenomena mentioned, it can be proposed the primary (SB1) and subsidiary (SB2) slip systems are originated by initial dislocation movements. The similar results were also found in Ref.[27].

(II). In the 2nd phase, the movement of slip systems results in significant generation and accumulation of stacking faults (SF1 and SF2, in Fig. 4b). Moreover, the SF1 and the SF2 have the certain angles with SB1 and SB2, respectively.

(III). Two different directions of the stacking faults extend and interdiffuse each other with the cumulative action of plastic deformation (Fig. 5(a))[28].

(IV). In the 4th phase, sustaining interdiffusion process (3rd phase) causes dislocation movements along the dislocation planes and cross slips, reflecting in a significant accumulation of dislocation structures in the form of DT (Fig. 5(b) and Fig. 5(c)), DW and DC (Fig. 5(d)). Such formation of dislocation structures is efficient at blocking slip at higher sliding strains [29,30].

(V). A further increasing amount of sliding strain results in the subdivision of original coarse grains into sub-grains with DT and DW forming their grain boundaries (Fig. 6(a)).

(VI). Owing to the repeated sliding, the sub-grains via the dislocation annihilation and formation of multiple shear bands are refined.

(VII). In the final phase, as proposed by Lu et al.[31,32], dynamic recrystallization takes place in the final grain refinement process (Fig. 6(b), 5 - 50nm). Severe plastic deformation (SPD) induced by sliding causes nucleation at grain boundary, and then the grains are refined. The new grains have few internal dislocations, whereas the dislocations accumulate accompanied the plastic deformations ring the sliding. The new nucleation is generated and the processes are repeated subjecting to the test until the grain refinement is being in a steady state.

In addition, the size of nano-grains keep in some extent in the final process of this phase when the dislocation achieve equilibrium between formation and annihilation [22]. According to the paper of Ref. [33], the grain refinement improves brass wear resistance, which shows a good fit to our test results in the dynamic stability stage.

5. Conclusions

The running-in tribological behavior of Pb-free brass under lubricant condition have been systematically investigated. In the initial stage, the COF decreasing is accompanied by the high wear rate at approximately 460 cycles and 1480 cycles respectively. The reason is that the sustaining dislocation pile-ups accumulation generates debris particles, and then lubricant invades the pits and the furrows formed by the peeling off debris particles to cause the COF to decrease. Then the sliding test enters the dynamic stability stage with considerably smaller scatter in the value (i.e. COF, roughness and real-time wear rate) and remained constant throughout the remainder of the test due to the equilibrium between the processes of strain hardening and recovery.

The Schipper value (3.05×10^{-6}) of the test is lower than the critical value, and therefore the test is in the boundary lubrication region. Meanwhile, the adhesive wear occurs with several furrows and pits on the wear track being observed. Severe shear plastic deformation in the surface layer of brass introduces dislocation movement, which give rise to cracks and voids. On the other hand, the void distribution in the sub-surface can accelerate the accumulation of dislocation near the surface.

Finally, a grain refinement mechanism during sliding experiment is proposed. The results confirm that two slip systems involve two stacking faults, which extend and interdiffuse each other, respectively. Moreover, sustaining interdiffusion process causes dislocation movement and accumulation, which contribute to the formation of complex random structures as DT, DW and DC. Increasing amounts of sliding strain results in sub-grains via the dislocation annihilation and formation of multiple shear bands, which eventually lead to a dynamic nano-grain structure with good wear resistance.

Acknowledgements

This work is funded by the National Natural Science Foundation of China（Project no. 51601021, 51441001）and the German Science Foundation DFG (Project no. DI 1494/4-1) and Natural Science Foundation of Jiangsu Province (Project no. BK20140262) and the Natural Science Foundation of Jiangsu Higher Education Institutions(17KJA460002) and China Postdoctoral Science Foundation (Project no. 2017M611718). The authors also wish to thank André Blockhaus for assistance with the in-situ tribological experiments.

References

1. Nobel, C., Hofmann, U., Klocke, F., Veselovac, D., Puls, H.: Application of a new, severe-condition friction test method to understand the machining characteristics of Cu–Zn alloys using coated cutting tools. Wear **344–345**, 58-68 (2015). doi:https://doi.org/10.1016/j.wear.2015.10.016
2. Liu, J., Wang, X.H., Ran, Q.N., Zhao, G., Zhu, X.X.: Microstructure and properties of Cu–3Ti–1Ni alloy with aging process. Transactions of Nonferrous Metals Society of China **26**(12), 3183-3188 (2016). doi:https://doi.org/10.1016/S1003-6326(16)64450-3
3. Bagheri, G.A.: The effect of reinforcement percentages on properties of copper matrix composites reinforced with TiC particles. Journal of Alloys and Compounds **676**, 120-126 (2016). doi:https://doi.org/10.1016/j.jallcom.2016.03.085
4. Lu, Z.C., Zeng, M.Q., Xing, J.Q., Zhu, M.: Improving wear performance of CuSn5Bi5 alloys through forming self-organized graphene/Bi nanocomposite tribolayer. Wear **364–365**, 122-129 (2016). doi:https://doi.org/10.1016/j.wear.2016.07.014
5. Feser, T., Stoyanov, P., Mohr, F., Dienwiebel, M.: The running-in mechanisms of binary brass studied by in-situ topography measurements. Wear **303**(1–2), 465-472 (2013). doi:https://doi.org/10.1016/j.wear.2013.03.047
6. Gane, N.: The effect of lead on the friction and machining of brass. Philosophical Magazine A **43**(3), 545-566 (2006). doi:10.1080/01418618108240394
7. Environmental Protection Agency: Safety of Public Water Systems – The Safe Drinking Water Act (SDWA), came into effect on 31.12.2002. Public Health Service Act.
8. European Parliament and Council: Directive 2000/53/EC on End of Life Vehicles (ELV), came into effect on 18.09.2000. Gazette of the European Community, 269, 2000, pp. 34–42.
9. European Parliament and Council: Directive 2011/65/EU on Restriction of Hazardous Substances (RoHS2), revised form came into effect on 08.06.2011.
10. Bundesministerium für Gesundheit, Verbraucherschutz, Ernährung und Landwirtschaft: Verordnung zur Novellierung der Trinkwasserverordnung (TrinkwV2001), came into effect on 21. 05. 2001. Bundesgesetzblatt 24, 2001, pp. 959-980.
11. Zambrano, O.A., Aguilar, Y., Valdés, J., Rodríguez, S.A., Coronado, J.J.: Effect of normal load on abrasive wear resistance and wear micromechanisms in FeMnAlC alloy and other austenitic steels. Wear **348–349**, 61-68 (2016). doi:https://doi.org/10.1016/j.wear.2015.11.019
12. Hernández Battez, A., González, R., Viesca, J.L., Fernández, J.E., Díaz Fernández, J.M., Machado, A., Chou, R., Riba, J.: CuO, ZrO2 and ZnO nanoparticles as antiwear additive in oil lubricants. Wear **265**(3–4), 422-428 (2008). doi:https://doi.org/10.1016/j.wear.2007.11.013
13. AsadiKouhanjani, S., ZareBidaki, A., Akbari, A.: The effect of sliding speed and amount of loading on friction and wear behavior of Cu–0.65 wt.%Cr alloy. Journal of Alloys and Compounds **486**(1–2), 319-324 (2009). doi:https://doi.org/10.1016/j.jallcom.2009.06.129
14. Dienwiebel, M., Pöhlmann, K.: Nanoscale Evolution of Sliding Metal Surfaces During Running-in.

Tribology Letters **27**(3), 255-260 (2007). doi:10.1007/s11249-007-9216-y

15. Nehl, E.: Wear test for bulk metal forming using a radionuclide technique. Wear **107**(4), 329-341 (1986). doi:https://doi.org/10.1016/0043-1648(86)90163-8
16. Trdan, U., Skarba, M., Grum, J.: Laser shock peening effect on the dislocation transitions and grain refinement of Al–Mg–Si alloy. Materials Characterization **97**, 57-68 (2014). doi:https://doi.org/10.1016/j.matchar.2014.08.020
17. Korres, S., Dienwiebel, M.: Design and construction of a novel tribometer with online topography and wear measurement. The Review of scientific instruments **81**(6), 063904 (2010). doi:10.1063/1.3449334
18. Scherge, M., Pöhlmann, K., Gervé, A.: Wear measurement using radionuclide-technique (RNT). Wear **254**(9), 801-817 (2003). doi:http://dx.doi.org/10.1016/S0043-1648(03)00230-8
19. Cao, H.M., Zhou, X., Li, X.Y., Lu, K.: Friction mechanism in the running-in stage of copper: From plastic deformation to delamination and oxidation. Tribology International **115**, 3-7 (2017). doi:http://dx.doi.org/10.1016/j.triboint.2017.05.027
20. Jahanmir, S., Suh, N.P., Abrahamson, E.P.: The delamination theory of wear and the wear of a composite surface. Wear **32**(1), 33-49 (1975). doi:http://dx.doi.org/10.1016/0043-1648(75)90203-3
21. P. Suh, N.: The delamination theory of wear. Wear **25**(1), 111-124 (1973). doi:10.1016/0043-1648(73)90125-7
22. Moshkovich, A., Perfilyev, V., Bendikov, T., Lapsker, I., Cohen, H., Rapoport, L.: Structural evolution in copper layers during sliding under different lubricant conditions. Acta Materialia **58**(14), 4685-4692 (2010). doi:https://doi.org/10.1016/j.actamat.2010.05.001
23. Moshkovich, A., Perfilyev, V., Meshi, L., Samuha, S., Cohen, S., Cohen, H., Laikhtman, A., Rapoport, L.: Friction, wear and structure of Cu samples in the lubricated steady friction state. Tribology International **46**(1), 154-160 (2012). doi:https://doi.org/10.1016/j.triboint.2011.03.013
24. Moshkovich, A., Perfilyev, V., Gorni, D., Lapsker, I., Rapoport, L.: The effect of Cu grain size on transition from EHL to BL regime (Stribeck curve). Wear **271**(9), 1726-1732 (2011). doi:http://dx.doi.org/10.1016/j.wear.2010.12.052
25. Tang, S.H., Wu, S., Kobayashi, M., Pan, H.L.: Effects of texture evolutions and point defects on ultrasonic waves under simple shear and pure shear. International Journal of Solids and Structures **44**(3–4), 1277-1290 (2007). doi:https://doi.org/10.1016/j.ijsolstr.2006.06.014
26. Lu, J.Z., Luo, K.Y., Zhang, Y.K., Sun, G.F., Gu, Y.Y., Zhou, J.Z., Ren, X.D., Zhang, X.C., Zhang, L.F., Chen, K.M., Cui, C.Y., Jiang, Y.F., Feng, A.X., Zhang, L.: Grain refinement mechanism of multiple laser shock processing impacts on ANSI 304 stainless steel. Acta Materialia **58**(16), 5354-5362 (2010). doi:http://dx.doi.org/10.1016/j.actamat.2010.06.010
27. Lychagin, D.V., Filippov, A.V., Novitskaia, O.S., Chumlyakov, Y.I., Kolubaev, E.A., Sizova, O.V.: Friction-induced slip band relief of -Hadfield steel single crystal oriented for multiple slip deformation. Wear **374–375**, 5-14 (2017). doi:https://doi.org/10.1016/j.wear.2016.12.028
28. Zhang, P., Qu, S., Yang, M.X., Yang, G., Wu, S.D., Li, S.X., Zhang, Z.F.: Varying tensile fracture mechanisms of Cu and Cu–Zn alloys with reduced grain size: From necking to shearing instability. Materials Science and Engineering: A **594**(Supplement C), 309-320 (2014). doi:https://doi.org/10.1016/j.msea.2013.11.079
29. Fischer, A.: Subsurface microstructural alterations during sliding wear of biomedical metals.

Modelling and experimental results. Computational Materials Science **46**(3), 586-590 (2009). doi:https://doi.org/10.1016/j.commatsci.2009.01.016

30. Christian Greiner, Z.L., Luis Strassberger, Peter Gumbsch: Sequence of stages in the microstructure evolution in copper under mild reciprocating tribological loading. ACS Applied Materials & Interfaces **8**, 15809-15819 (2016).
31. Lu, J.Z., Luo, K.Y., Zhang, Y.K., Cui, C.Y., Sun, G.F., Zhou, J.Z., Zhang, L., You, J., Chen, K.M., Zhong, J.W.: Grain refinement of LY2 aluminum alloy induced by ultra-high plastic strain during multiple laser shock processing impacts. Acta Materialia **58**(11), 3984-3994 (2010). doi:https://doi.org/10.1016/j.actamat.2010.03.026
32. Karthikeyan, S., Agrawal, A., Rigney, D.A.: Molecular dynamics simulations of sliding in an Fe–Cu tribopair system. Wear **267**(5), 1166-1176 (2009). doi:http://dx.doi.org/10.1016/j.wear.2009.01.032
33. Zhai, W.Z., Shi, X.L., Wang, M., Xu, Z.S., Yao, J., Song, S.Y., Wang, Y.F.: Grain refinement: A mechanism for graphene nanoplatelets to reduce friction and wear of Ni3Al matrix self-lubricating composites. Wear **310**(1-2), 33-40 (2014). doi:10.1016/j.wear.2013.12.014